

RECOVER: sequential model optimization platform for combination drug repurposing identifies novel synergistic compounds *in vitro*

Paul Bertin¹, Jarrid Rector-Brooks¹, Deepak Sharma¹, Thomas Gaudet², Andrew Anighoro², Torsten Gross², Francisco Martínez-Peña³, Eileen L. Tang³, Suraj M S², Cristian Regep², Jeremy Hayter², Maksym Korablyov¹, Nicholas Valiante⁴, Almer van der Sloot⁵, Mike Tyers⁵, Charles Roberts², Michael M. Bronstein^{6,7}, Luke L. Lairson³, Jake P. Taylor-King², and Yoshua Bengio¹

¹ Mila, the Quebec AI Institute, Canada ² Relation Therapeutics, London, UK

³ Department of Chemistry, The Scripps Research Institute, USA ⁴ Glyde Bio, Inc, USA.

⁵ IRIC, Institute for Research in Immunology and Cancer, Université de Montréal, Canada

⁶ Department of Computer Science, University of Oxford, UK ⁷ Twitter, UK

jake@relationrx.com, yoshua.bengio@mila.quebec

ABSTRACT

Selecting optimal drug repurposing combinations for further preclinical development is a challenging technical feat. Due to the toxicity of many therapeutic agents (e.g., chemotherapy), practitioners have favoured selection of synergistic compounds whereby lower doses can be used whilst maintaining high efficacy. For a fixed small molecule library, an exhaustive combinatorial chemical screen becomes infeasible to perform for academic and industry laboratories alike. Deep learning models have achieved state-of-the-art results *in silico* for the prediction of synergy scores. However, databases of drug combinations are highly biased towards synergistic agents and these results do not necessarily generalise out of distribution. We employ a sequential model optimization search applied to a deep learning model to quickly discover highly synergistic drug combinations active against a cancer cell line, while requiring substantially less screening than an exhaustive evaluation. Through iteratively adapting the model to newly acquired data, after only 3 rounds of ML-guided experimentation (including a calibration round), we find that the set of combinations queried by our model is enriched for highly synergistic combinations. Remarkably, we rediscovered a synergistic drug combination that was later confirmed to be under study within clinical trials. Our method is available at: <https://github.com/RECOVERcoalition/Recover>.

1 INTRODUCTION

Drug combinations are an important therapeutic strategy for treating diseases that are subject to evolutionary dynamics, in particular cancers and infectious disease [1, 2]. Conceptually, as tumours or pathogens are subject to change over time, they may develop resistance to a single agent [3] – motivating one to target multiple biological targets simultaneously [4]. Discovering synergistic drug combinations is an important step towards developing robust therapies as they hold the potential for greater efficacy, reducing dose and thereby limiting the likelihood of adverse effects. There are approximately 20,000 proteins encoded by the human genome alone and many pathogenic targets beyond this. More concretely, in a drug repurposing scenario (i.e., uncovering new indications for known drugs), a small molecule library of >4,000 FDA approved drugs [5] leads to >8 million pairwise combinations; this does not appear tractable with standard high throughput screening (HTS) technology – even at a single dose [6].

With the recent COVID-19 global health crisis, there has been the need for rapid drug repurposing that would allow for expedited and de-risked clinical trials. Due to the complexity of selecting drug combinations and minimal training data publicly available, studies have typically been focused towards monotherapy repurposing from a variety of angles – often involving artificial intelligence (AI) techniques to provide recommendations [7]. Pioneering work,

often utilizing deep learning, has now led to the prediction of synergistic drug combinations in a systematic manner. However, there is a dearth of drug combination datasets due to the large combinatorial space of possible experiments – ultimately limiting the quality of such predictions. A cost-efficient solution involves the use of sequential model optimization (SMO) where one performs both informative experiments (“*exploration*”) and experiments that double-down on a promising hypothesis (“*exploitation*”) [8]. Utilisation of such approaches can result in discovering most of the promising combinations within a given library while requiring substantially less experimentation than an exhaustive search. With an SMO platform available in conjunction with an appropriate *in vitro* assay, one has a powerful tool to rapidly respond to a future public health crisis.

There have now been a number of approaches for selection of drug combinations [9]. Classic bioinformatics approaches have focused on using machine learning and network statistics over specified features of drugs (e.g., molecular fingerprints [10]), cell lines (e.g., transcriptomics, copy number variations [11]) and interactome topology between biomolecules (e.g., protein–protein interactions, gene regulatory networks [12]). Initiatives such as the Dialogue on Reverse Engineering Assessment and Methods (DREAM) have led to a plethora of methods being benchmarked against one another in prospective challenges through the generation of novel datasets [13]. Relevant to searching through large

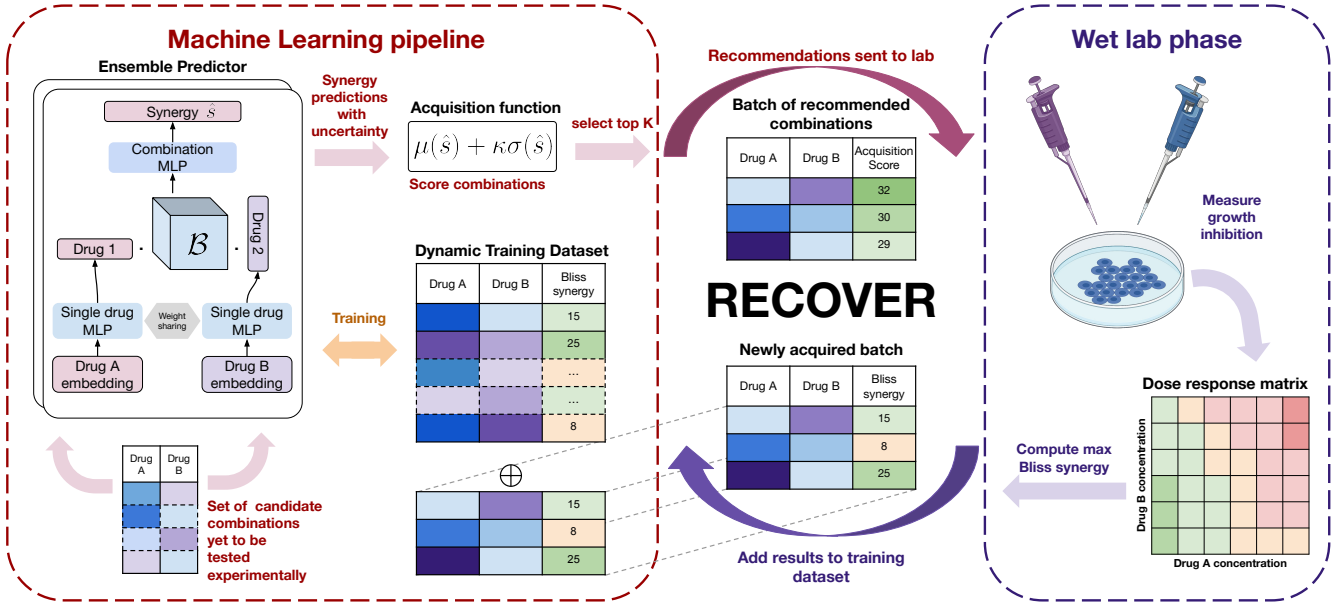


Figure 1: Overview of the RECOVER workflow integrating both a novel machine learning pipeline and iterated wet lab evaluation.

combinatorial spaces, complex deep learning architectures have been used to predict both adverse drug-drug interactions [14, 15] and synergistic drug combinations [16–18]. SMO has shown huge promise across a number of areas in biology, e.g., identification of inhibitors of *Mycobacterium tuberculosis* growth [19], but has not yet been applied in the context of drug combination selection for repeated experiments.

We present a sequential model optimization platform that can guide wet lab experiments: RECOVER. We first propose a *synergy regressor* model based on a novel symmetric deep learning architecture. This regressor estimates the synergy for an arbitrary pair of drugs represented through their molecular fingerprints. We perform a retrospective validation to benchmark the performance of our model using the DrugCombin database which is focused on oncology data [20]. Thereafter, we evaluate our SMO pipeline *in silico*, which allows the model to select the most relevant data points to be labelled in order to discover most promising combinations while reducing model uncertainty. Finally, we test RECOVER prospectively in an *in vitro* experimental setting whereby we discover novel synergistic combinations active against a breast cancer model cell line (MCF7). This forms a proof of concept demonstration of RECOVER – which then justifies the investment in a much larger drug combination screen.

2 RESULTS

2.1 RECOVER: sequential model optimization platform for rapid drug repurposing

RECOVER is an open-source SMO platform for the optimal suggestion of drug combinations, see Figure 1. To encourage use by the scientific community, we detail a configuration that can be trained

on a personal computer or laptop without requiring dedicated computational infrastructure. Pairs of drug feature vectors are fed into a deep neural network which is used for the prediction of synergy scores. These feature vectors include molecular fingerprints as well as a one-hot encoding identifying a drug. For a description of the model, see Section 3.

Our core focus is the prediction of pairwise drug combination synergy scores. Whilst many mathematical descriptions of synergy have been proposed, in the following work, we utilise the Bliss synergy score due to its simplicity and numerical stability. In the context of cell viability, the Bliss independence model assumes that in the absence of synergistic effects, the expected fraction of viable cells after treatment with drugs *a* and *b* at doses *c_a* and *c_b*, written *V(c_a, c_b)*, is identical to the product of the fractions of viable cells when utilising each drug independently, i.e., *V(c_a)V(c_b)*. We then define the Bliss synergy score as the difference between these quantities such that a fraction of surviving cells *V(c_a, c_b)* smaller than the expected proportion *V(c_a)V(c_b)* leads to a large Bliss synergy score

$$s_{Bliss}(c_a, c_b) = V(c_a)V(c_b) - V(c_a, c_b) \tag{1}$$

$$= I(c_a, c_b) - I(c_a) - I(c_b) + I(c_a)I(c_b), \tag{2}$$

where *I(·) = 1 - V(·)* is the experimentally measured growth inhibition induced by drug *a*, *b*, or both together at the associated doses. Given a dose-response matrix for the two drugs, a global synergy score can be obtained through a pooling strategy. In our case, we take the maximum value, i.e.,

$$\hat{s}_{Bliss} = \max_{c_a, c_b} s_{Bliss}(c_a, c_b). \tag{3}$$

In many studies, the arithmetic mean is taken to calculate a global synergy score. Unfortunately, different laboratories use different

RECOVER: sequential model optimization platform for combination drug repurposing identifies novel synergistic compounds *in vitro*

dose intervals for each drug, and typically each drug combination shows a synergistic effect at a specific dose-pair interval. Therefore, the arithmetic mean is highly sensitive to the chosen dose interval, which is why we chose to prioritise a max-pooling strategy as in Eq. 3. Unless explicitly stated otherwise, a synergy score refers to a global max-pooled Bliss score.

In addition to the prediction of synergy, our model estimates the uncertainty associated with the underlying prediction. More precisely, for a given combination of drugs, our model does not only provide a point estimate of the synergy, but estimates the distribution of possible synergy scores for each combination, which we refer to as the *predictive distribution*. We define the uncertainty as the standard deviation of the predictive distribution.

An acquisition function [21] is used to select the combinations that should be tested in subsequent experiments. This acquisition function is selected to balance between: *exploration*, prioritising combinations with high uncertainty whereby labelling said points should increase predictive accuracy; and *exploitation*, selection of combinations believed to be synergistic with high confidence. Through using a balanced method, it is believed that performance across many experimental rounds is superior to an exploration-only or exploitation-only strategy.

In summary, our SMO setting consists of generating recommendations of drug combinations that will be tested *in vitro* at regular intervals. At each step, our model is trained on all the data acquired up to that point, and predictions are made for all combinations that could be hypothetically tested experimentally. The acquisition function is then used to provide recommendations for *in vitro* testing. The results of the experiments are then added to the training data for the next round of experiments and the whole process repeats itself.

2.2 Retrospective testing of RECOVER rapidly predicts and rediscovers synergistic drug combinations

We first evaluate the performance of our model *in silico*. After comparing RECOVER to simple baselines, we investigate the generalization abilities of the model in order to understand the scope of tasks to which it can be applied. Finally, we evaluate performance in the context of Sequential Model Optimization.

Due to the limited size of most individual drug combination studies reported in the literature, we focus on the NCI-ALMANAC viability screen [22] summarised in Figure 2. Unless explicitly stated otherwise, presented *in silico* benchmarking utilises this resource.

Moreover, we refrained from combining multiple datasets due to the severe batch effects between studies. In Figure 2E, we show a scatter plot demonstrates inconsistency between the O’Neil 2016 [23] series of drug combination experiments against their NCI-ALMANAC counterpart. We note this may be somewhat due to variation in the readouts of these experiments, but do not speculate further. Additional details of the data cleaning process are presented in Section 3.4.

2.2.1 RECOVER outperforms baseline models. We first benchmark the ability of RECOVER to predict synergy scores on a publicly available dataset. We compare our approach to several baseline models

for the prediction of the Bliss synergy score on the MCF7 cell line. We restrict ourselves to MCF7 for consistency with prospective *in vitro* experiments.

In Table 1, we demonstrate that RECOVER outperforms baseline models in terms of R^2 and Spearman correlation metrics. The hyperparameters for each model are optimized using a grid search; extended details regarding the optimization procedure can be found in Appendix A.1.

	R^2	Spearman corr.
RECOVER	0.242 ± 0.006	0.466 ± 0.007
Linear SVM	0.171 ± 0.01	0.453 ± 0.004
Gradient Boosting Trees	0.172 ± 0.002	0.459 ± 0.001

Table 1: Comparison of RECOVER with baseline models for the synergy score prediction within the MCF7 cell line. Standard deviation computed over 3 seeds.

We note that whilst performance appears modest, we argue that this results from experimental noise in addition to the non-uniform distribution of synergy scores. In Appendix B, we compute an upper bound for the performance of the regression model in relation to the magnitude of noise from experimental observations. We then estimate the level of noise in the NCI-ALMANAC data set, and compare the performance of RECOVER to the estimated best achievable performance. This analysis shows that the RECOVER model performance is reasonably close to the hypothetical maximum; for example, RECOVER achieves 0.47 Spearman correlation, while the highest achievable Spearman correlation is estimated to be 0.64.

We now provide some evidence that this level of predictability can in fact be sufficient within a Sequential Model Optimization setting to identify highly synergistic combinations. We do this through recovery of the top fraction of highly synergistic combinations — defined by a maximum Bliss synergy score of above 30 — within the test set. In Figure 3, we report the proportion of highly synergistic combinations as a function of the number of combinations queried. The percentage of synergistic combinations in the query is superior to the proportion in the whole test set, but decreases with the size of the query.

Exemplar visualizations of the drug embeddings learnt by RECOVER are available in Appendix C.1.

2.2.2 Generalization capabilities of RECOVER. We have shown that predictions from RECOVER can be used to identify highly synergistic drug combinations retrospectively given a cell line and a fixed set of drugs. We now investigate whether RECOVER can generalize beyond the training distribution in various ways: (a.) What is the performance on test examples drawn from the same distribution as the training set was drawn from? (b.) Can RECOVER generalize to new drugs? (c.) Can RECOVER leverage observations from other cell lines in order to improve the predictions on the MCF7 cell line? (d.) Can RECOVER predict the synergy of a combination on the MCF7 cell line if this combination has already been tested on other cell lines? (e.) Can RECOVER predictions transfer to new experimental scenarios? These tasks are illustrated graphically in Figure 4. Answering these questions is crucial to aid experimental design in a prospective setting.

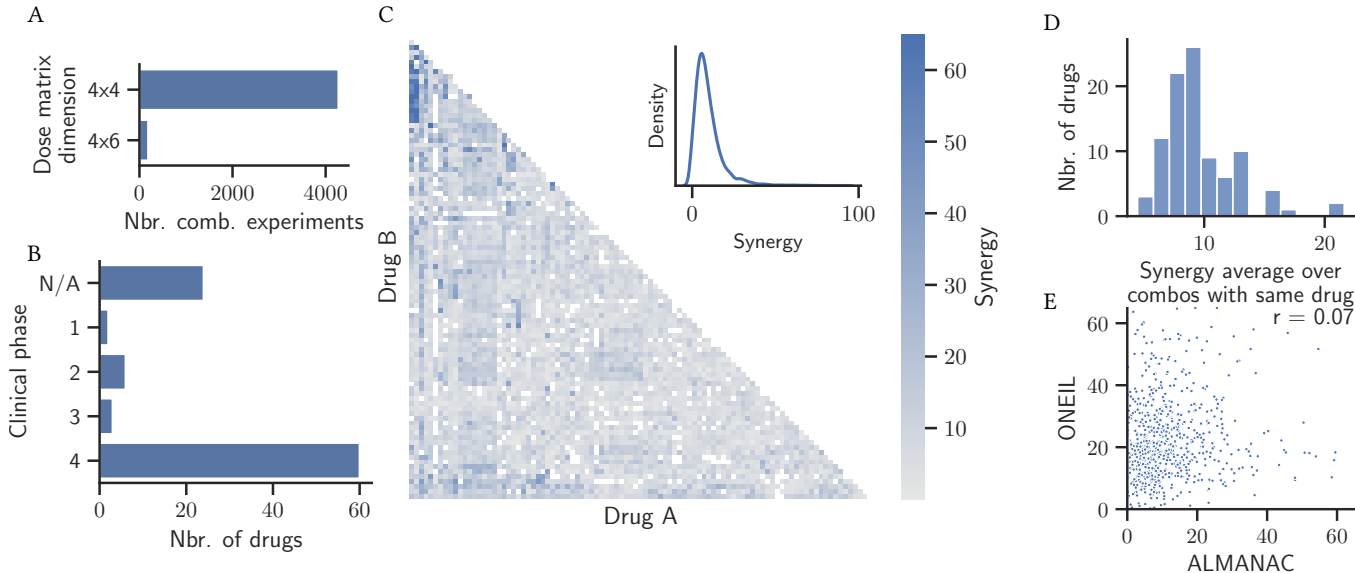


Figure 2: Model performance was evaluated on synergy data from the NCI-ALMANAC viability screen [22] for the MCF7 cell line. After quality control, synergy scores could be computed for 4271 unique drug pairs. (A.) Distribution of dose-response matrix dimensions. (B.) Distribution of clinical phases of the considered 95 distinct drugs. (C.) Synergy scores for each drug-pair. White squares indicate missing or removed (low-quality) dose-response matrices. (D.) Histogram of average synergy scores for each drug computed across all drug pairs recorded. (E.) Scatter plot across 783 (drug-pair, cell line) tuples found in both NCI-ALMANAC and O’Neil 2016 [23].

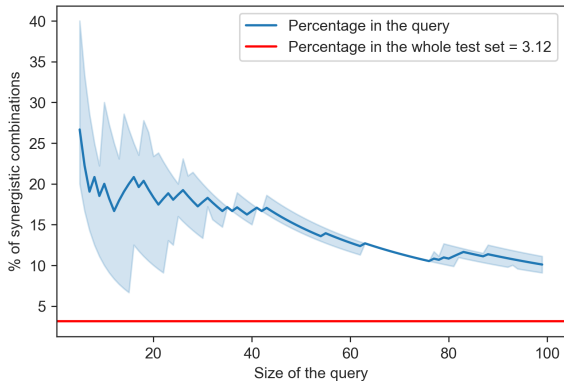


Figure 3: Proportion of queried combinations with synergy score >30 in test set as a function of query size (MCF7 cell line data). Standard deviation computed over 3 seeds.

Depending on the task at hand, the model configuration will differ slightly. For all tasks (excluding the *drug level split* task), the drug feature representations consists of the Morgan fingerprints [24] concatenated with a one-hot encoding of the drug. For the *drug level split* task, only the Morgan fingerprint is used. When several cell lines are available, the model is conditioned on cell lines using feature-wise linear modulation (FiLM) [25]. The cell line features are either a one-hot encoding of the cell line for tasks (c.) and (e.), or some information about mutations and basal level of gene expression for task (d.). For more details refer to Section 3.4.

In Table 2, we report the validation and test performance metrics of RECOVER for each of the five tasks. This analysis provides several key insights. First, we notice that there is a significant drop in performance when trying to generalize to combinations of new drugs. However performance is still above the level of random selection – as confirmed by Figure 13 available in Appendix. Second, we notice that leveraging other cell lines improves performance on the MCF7 cell line in terms of R^2 , and the synergy of a combination can be well predicted on MCF7 if it has already been observed for other cell lines. Finally, we notice that the model generalizes poorly to an entirely new experimental setting. From Figure 2E, this appears to be due to severe batch effects.

For prospective *in vitro* experiments, this analysis suggests a staged approach is required to adapt our model to a new laboratory and then to novel compounds.

2.2.3 Backtesting RECOVER demonstrates efficient exploration of drug combination space. We benchmarked the SMO pipelines as described in Section 2.1, whereby the model is shown a fraction of the full data set and can choose sample points to unblind. This analysis is restricted to the MCF7 cell line.

In order to simulate real-world interactions with the wet lab, we start with a set of 30 randomly chosen drug pairs that the pipeline is initially trained on, while the rest of the data is hidden from the pipeline. Hence, these combinations are always part of the visible set. We split the visible set into a training and validation set (80/20), train the model using early stopping and then acquire 30 additional drug pairs, before repeating the entire procedure again with the new training set of 60 drug pairs (i.e., 30 + 30), and then with 90,

RECOVER: sequential model optimization platform for combination drug repurposing identifies novel synergistic compounds *in vitro*

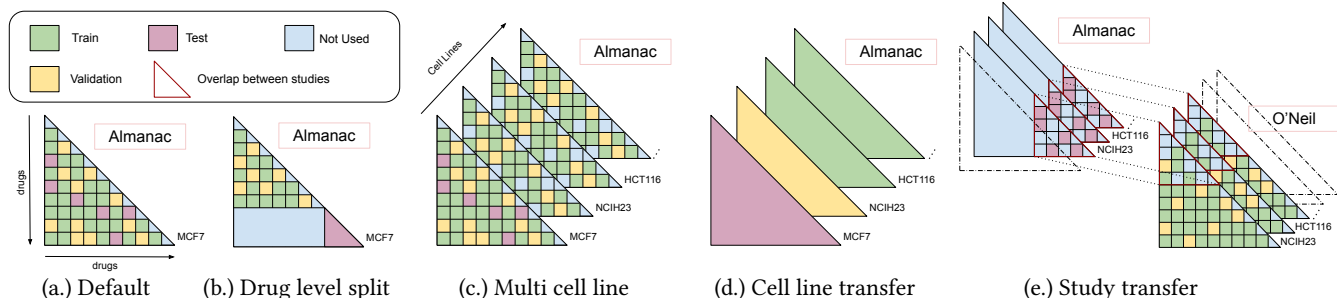


Figure 4: Overview of the different tasks on which RECOVER has been evaluated. Each task corresponds to a different way to split the training, validation and test sets, and aims at evaluating a specific generalization ability of the model. **(a.)** Default. Combinations are split randomly into training/validation/test (70%/20%/10%). Only the MCF7 cell line is used. **(b.)** Drug Level Split. The test set consists of combinations among drugs that are excluded from the training and validation sets. 30% of available drugs are used for test. Remaining combinations are split into training and validation (80%/20%). Only the MCF7 cell line is used. **(c.)** Multi Cell Line. All cell lines are used for training and validation, but the test set is restricted to the MCF7 cell line. If a combination is part of the test set, it is never used in the training and validation sets, regardless of cell line. Training/validation split is consistent across cell lines. Proportions (70%/20%/10%) **(d.)** Cell Line Transfer. The test set consists of all examples corresponding to the MCF7 cell line. Other cell lines are randomly assigned to training/validation (80%/20%). A given combination can appear in both training and test sets **(e.)** Study Transfer. The O’Neil 2016 study [23] is used to generate the training and validation sets. All overlapping cell lines are used. NCI-ALMANAC is used to generate the test set. The test set is restricted to combinations for which both drugs also appear in the O’Neil study. If a combination is part of the test set, it is excluded from training and validation sets, regardless of cell line.

		(a.) Default	(b.) Drug Level Split	(c.) Multi Cell Line	(d.) Cell Line Transfer	(e.) Study Transfer
R^2	Valid.	0.343 ± 0.053	0.401 ± 0.147	0.387 ± 0.032	0.278 ± 0.027	0.304 ± 0.021
	Test	0.242 ± 0.006	0.038 ± 0.002	0.282 ± 0.017	0.382 ± 0.017	0.014 ± 0.016
Spearman c.	Valid.	0.474 ± 0.021	0.459 ± 0.069	0.518 ± 0.021	0.299 ± 0.047	0.589 ± 0.032
	Test	0.466 ± 0.007	0.157 ± 0.012	0.448 ± 0.021	0.378 ± 0.015	0.147 ± 0.075

Table 2: Performance of RECOVER for the different tasks, as detailed in Figure 4. Standard deviation computed over 3 seeds.

and so on, until no more drug pairs are left to acquire from the hidden set.

A range of methods can be used to generate recommendations for new drug pairs, typically as specified by an *acquisition function* [21]. The acquisition functions that we investigate are detailed in Section 3.2.2.

Our *in silico* experiments try to mirror as closely as possible the setting of the *in vitro* experiments. Therefore, unless specified otherwise, they were restricted to the MCF7 cell line and 30 combinations were acquired at a time using the same model as the one used to generate recommendations for the *in vitro* experiments.

We compare acquisition functions by the rate at which they unblind the set of top 1% of synergistic combinations in the NCI-ALMANAC dataset within each synthetic experimental round (or *iteration*). As shown in Figure 5, Greedy acquisition and Upper Confidence Bound (UCB) acquisition, two Model-based searches, perform on par with each other and outperform Random Search by a large margin. Both approaches discover 80% of the top 1% of synergistic drug pairs in approximately 15 iterations whereas Random Search discovers less than 20%.

We note that for the prediction of the average Bliss synergy score (instead of the maximum Bliss) using a configuration with a smaller

batch size (5 drugs per iteration), described in Appendix D.1, UCB outperformed the Greedy acquisition function, see Figure 5 (inset). This demonstrates that taking uncertainty into account to guide experiments can increase the performance of the pipeline over a naive Greedy acquisition strategy in some cases.

Figure 6 presents the average synergy among queried combinations at each step of the SMO pipeline. While the average synergy using Random Search is always approximately 10, Model-based searches query batches for which the average synergy can be up to 25. After approximately 15 iterations, the average synergy in the queries starts to decrease, as there are very few highly synergistic combinations left to query.

Another important aspect of the SMO pipeline is its ability to leverage publicly available data in order to improve performance in a new experimental setting. To this end, we analyzed the impact of pretraining the model on the O’Neil database before simulating SMO experiments on a subset of the NCI-ALMANAC database. As shown in Figure 7, pretraining improves SMO performance, meaning that knowledge can be transferred from one study to the other, even though model predictions do not generalize *without adaptation*, see Appendix D.2 for details.

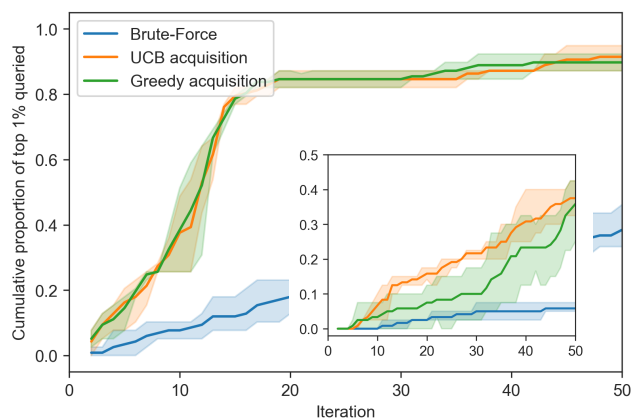


Figure 5: Cumulative proportion of the top 1% synergistic combinations that have been rediscovered by RECOVER using the model configuration described in the main text. (inset) UCB can outperform Greedy acquisition in certain model configurations, detailed in Appendix D.1. Standard deviation computed over 3 seeds.

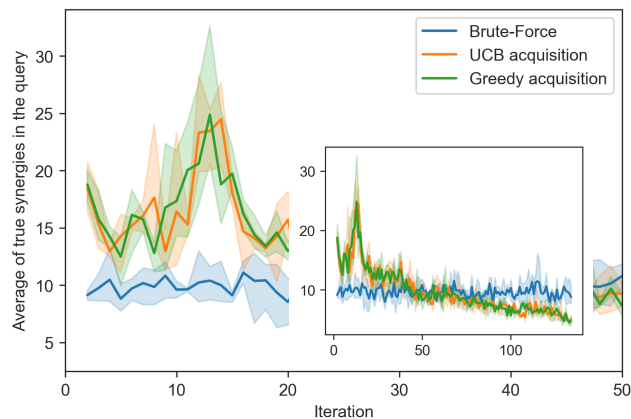


Figure 6: Average of the true synergies of the drug pairs that have just been queried at each step of the SMO pipeline. (inset) Zoomed out view. Standard deviation computed over 3 seeds.

2.3 Prospective use of RECOVER enriches for selection of synergistic drug combinations

From the *in silico* results, we now test RECOVER prospectively in an oncology setting, leveraging publicly available data to pretrain upon. The MCF7 cell line was used to generate 6×6 dose-response matrices, see Section 3.5 for more details. We perform multiple rounds of RECOVER-informed wet lab experiments and observe sequential improvements in performance. The rounds of experiments are described as follows:

1. Calibration. The initial round of experiments is used to supplement publicly available data with 20 randomly selected

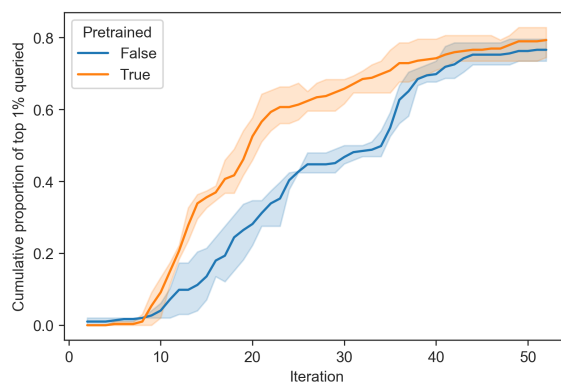


Figure 7: Effect of pretraining on the rate of discovery of highly synergistic combinations within NCI-ALMANAC through pretraining on O’Neil. SMO performed on the subset of NCI-ALMANAC consisting of drug pairs for which at least one drug is contained within O’Neil. Only cell lines appearing in both studies were used and RECOVER was conditioned on cell line. Standard deviation computed over 3 seeds

unseen drug combinations. Furthermore, we confirmed the previous *in silico* result that we could not predict synergy scores for unseen drugs (using public data) through selecting the 5 top combinations selected by RECOVER and a Graph Neural Network (GNN) model that we did not pursue further. It was also specified that drug should appear in at most a single drug combination queried.

2. Diversity. We now select drug combinations based on the model predictions through the UCB acquisition function. To further ensure that we quickly observe all single drugs at least once (as we showed that the model cannot generalize well to unseen drug combinations), we select our batch of experiments as follows. First we rank combinations according to their acquisition function score. We then find the first combination which involves a drug that has not yet been used (or involved in one of the combinations from the current batch), and add it to the batch. We repeat until we have 30 combinations in the batch.

3. SMO Search. RECOVER is now free to select any drug pairs of interest for testing, with the requirement that any single drug may be selected no more than 5 times.

The computational protocol was designed to predict synergy of drug pairs where only one compound was already seen by the model during pretraining on ALMANAC, see grey area in Figure 8A. NCI-ALMANAC includes 95 unique drugs which were employed in combinations tested on MCF7 cell line. We chose to deprioritise drugs without a well-characterised mechanism of action (MoA) to facilitate biological interpretation and validation of the results, see pink area in Figure 8A. To achieve this, drugs in NCI-ALMANAC were annotated with known targets extracted from the ChEMBL drug mechanism table: 54 drugs matched with at least one known

RECOVER: sequential model optimization platform for combination drug repurposing identifies novel synergistic compounds *in vitro*

target were thus selected. An additional 54 drugs were selected by clustering drugs with known MoA that are included in the DrugComb [20] database but not in NCI-ALMANAC, see Section 3.4 for details. Hence, a search space including a total of 2,916 drug combinations were obtained, see the white area in left bottom corner of Figure 8A.

In Figure 8B, we plot the cumulative density function of each experimental round. We note that the distribution starts developing a heavier tail towards high max Bliss synergy scores and the mean synergy score significantly increases between the first to the third round (t -test, $p < 0.05$). This emergent heavy tail appears significant when comparing the distribution in the SMO Search round to the background distribution of synergy scores in NCI-ALMANAC (Kolmogorov–Smirnov test, $p < 0.025$), see Figure 2C (inset). Finally, the highest max Bliss synergy score observed increases from one round to the next.

The results of *in silico* experiments presented in Figure 6 suggest that performance may further increase in the following rounds of *in vitro* testing.

2.4 Discovery and rediscovery of novel synergistic drug combinations

We now discuss some of the key combinations identified, namely two highly synergistic combinations discovered in the SMO Search round: (a.) Alisertib & Pazopanib, and (b.) Flumatinib (mesylate) & Mitoxantrone (dihydrochloride). We plot the Bliss synergy matrices in Figure 9.

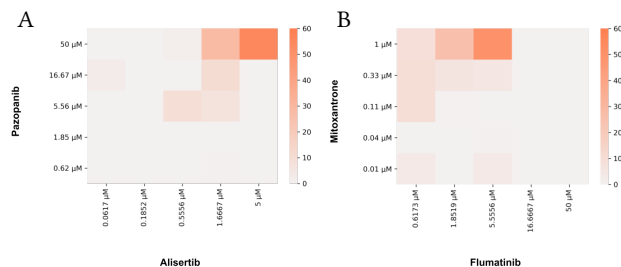


Figure 9: Bliss synergy dose response plots for (A.) Alisertib & Pazopanib and (B.) Flumatinib & Mitoxantrone.

Pazopanib inhibits angiogenesis through targeting a range of kinases including vascular endothelial growth factor receptor (VEGFR), platelet-derived growth factor receptor (PDGFR), c-KIT and fibroblast growth factor receptors (FGFR); in contrast Alisertib is a highly selective inhibitor of mitotic Aurora A kinase. Synergism between the two agents is hypothesised to be linked to the observation that mitosis-targeting agents also demonstrate antiangiogenic effects. In an independent study, the combination of Alisertib & Pazopanib has successfully completed phase 1b clinical trials for advanced solid tumours sponsored by the Takeda Pharmaceutical Company [26].

The combination of Flumatinib and Mitoxantrone appears to be linked to a similar mechanism, but does not seem to have been

studied in the biomedical literature. Whilst Flumatinib is a tyrosine kinase inhibitor targeting Bcr-Abl, PDGFR and c-KIT, Mitoxantrone is a Type II topoisomerase inhibitor. Furthermore, compared to the first combination, neither drug requires a high dose of 50 μM to achieve the maximum Bliss synergy score.

Our ability to prospectively identify highly synergistic drug combinations with orthogonal evidence whilst only testing fewer than 100 drug combinations suggests that SMO-driven drug combination screening should play a large role in future drug combination research. Furthermore, tools like RECOVER may have a role to play when addressing novel emergent infectious disease such as the COVID-19 pandemic.

3 METHODS

3.1 High level overview

We frame the problem of pairwise drug synergy prediction as a regression task $((a, b), \text{syn})$. Given a pair of drugs a, b , we aim to predict their level of synergy, syn . Our proposed architecture is an end-to-end framework trained with a *mean square error* (MSE) criterion.

Our model can be decomposed into two modules. First, a *single drug* module, E , which produces representations (or embeddings) for the drugs based on their chemical structure information. The embeddings from a pair of drugs is used as input to the *combination* module P , which directly estimates the synergy score; see Figure 10.

Further, uncertainty estimation methods are used in order to estimate the *predictive distribution* of synergies $p(\text{syn}|a, b)$ for each drug pair $\{a, b\}$, as opposed to a point estimate. The predictive distributions of drug pairs are given as input to an acquisition function in order to decide which combinations should be tested *in vitro*, balancing between combinations that are informative, *i.e.* that can reduce the generalization error of the model later on, and combinations that are likely to be synergistic.

3.1.1 Single drug module. Let $X_{\mathcal{D}} \in \mathbb{R}^{n_{\mathcal{D}} \times l_{\mathcal{D}}}$ denote the matrix of drug features, where $n_{\mathcal{D}}$ is the number of drugs in \mathcal{D} and $l_{\mathcal{D}}$ corresponds to the number of raw features that describe each drug. Drug features used in this work include molecular fingerprints [10] and one-hot encoding of the drugs.

We denote the matrix of cell line features by $X_C \in \mathbb{R}^{n_C \times l_C}$, with C the set of cell lines, n_C corresponding to the number of cell lines in C and l_C giving the number of raw features for each cell line.

The single drug module can be written as a function $E : \mathcal{D} \rightarrow \mathbb{R}^{k_{\mathcal{D}}}$ where $k_{\mathcal{D}}$ corresponds to the dimension of the output vector representation of each drug. Our single drug module is a simple multi-layer perceptron (MLP) that takes raw features of drugs as input and outputs an updated vector representation. This MLP can be conditioned on cell line as described in Section 3.1.3.

In Appendix A.2, we investigated several types of input features for the drugs. Best performance was achieved when using both Morgan fingerprints and one-hot encodings.

3.1.2 Combination module. Given a set of drugs \mathcal{D} , the combination module corresponds to a function $P : \binom{\mathcal{D}}{2} \mapsto \mathbb{R}$ that maps a pair of drugs to their Bliss synergy score. We remark first that P

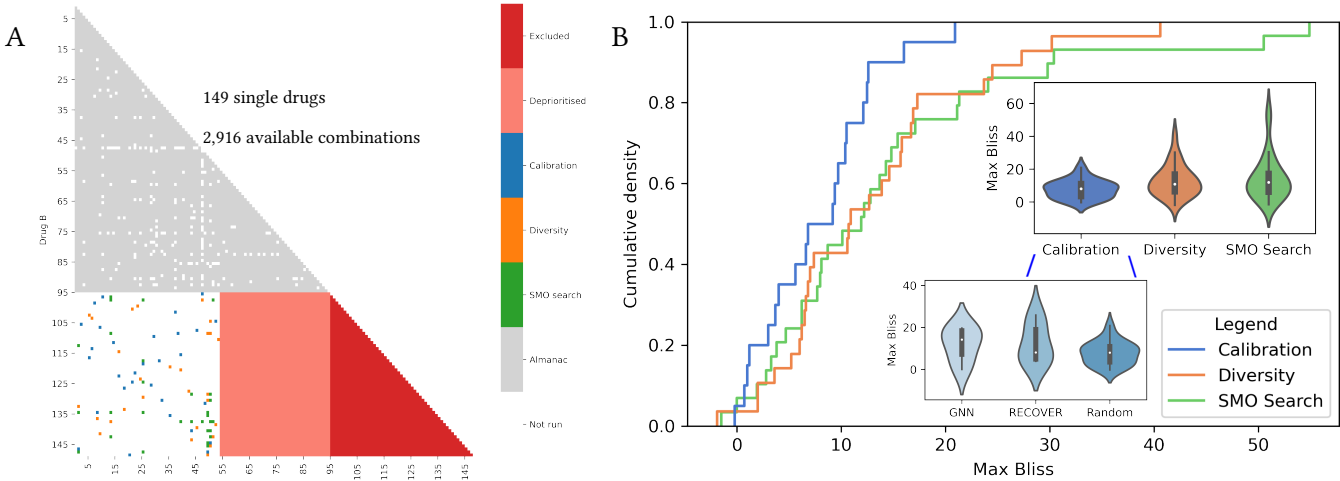


Figure 8: Prospective use of RECOVER for *in vitro* evaluation. (A.) Heatmap representing drug combinations used during pretraining (NCI-ALMANAC), in three subsequent experiment rounds, and excluded from the analysis. Drug combinations which were not available for pretraining or were not selected for experiments are represented in white. (B.) Cumulative density plot of max Bliss synergy score for each experimental round.

should be agnostic to the order of the two drugs. Hence, the first operation of P correspond to a permutation invariant function – such as element-wise sum, mean, or max operations – applied to the two vector representations corresponding to each drug. In this work, we use a bilinear operation defined by a tensor $B \in \mathbb{R}^{k_D \times k_D \times k}$, where k is a hyperparameter corresponding to the dimension of the vector representation of a drug combination. To ensure permutation invariance, we enforce that every slice across the third dimension (denoted as B_i), is a symmetric matrix. Note that we do not enforce B_i to be positive definite, hence B_i does not necessarily define a scalar product. The output of this permutation invariant function is fed to an MLP that outputs the predicted synergy for the pair of drugs. Again, the MLP can be conditioned on cell lines, see Section 3.1.3.

3.1.3 Cell line conditioning. As a drug effect is context dependent, the synergy of a combination of two drugs can be different in experiments using different cell lines. To account for the cell line in our model we condition on it using FiLM [25]. In essence, the FiLM approach learns an affine transformation of the activation of each neuron in the MLP.

The feature representation of the cell line is either based on a one-hot encoding, or on information about mutations and basal level of gene expression. The former approach relies on having data for each cell line in the training set and cannot generalise to new cell lines. The second approach makes use of features that represent cell lines as described in Section 3.4.

3.2 Searching the space of drug combinations

3.2.1 Uncertainty estimation. Estimating the uncertainty of the predictions is a key step towards providing reliable recommendations as well as driving the exploration with SMO. For this purpose,

we use a common uncertainty estimation methods, deep ensembles [27]. Given an ensemble of models which differ only in the initialization of the parameters, the predictions of the different models are considered as samples from the *predictive* distribution. In this work, we define uncertainty as the standard deviation of the *predictive* distribution, and can be estimated from the standard deviation between the predictions of the different members of the ensemble. Unless specified otherwise, we use a deep ensemble as the uncertainty estimation method in our experiments.

We also investigated directly estimating the standard deviation of the predictive distribution, in a similar fashion to DEUP [28]. Two models are initialized: the first one, denoted as the *mean predictor*, predicts the expected synergy $\hat{\mu}$ and is trained with Mean Square Error (MSE). The second model, denoted as the *uncertainty predictor*, outputs an estimate of the standard deviation of the predictive distribution $\hat{\sigma}$ and is trained to minimize the following negative log-likelihood criterion:

$$NLL = \frac{\log(\hat{\sigma}^2)}{2} + \frac{(y - \hat{\mu})^2}{2\hat{\sigma}^2}, \tag{4}$$

where y is the ground truth variable of interest. This criterion allows us to get an estimator $\hat{\sigma}$ of the standard deviation of the *predictive* distribution for each combination, and its derivation is presented in Appendix E. When fixing $\hat{\sigma} = 1$, NLL corresponds to the MSE criterion.

3.2.2 Sequential model optimization. Sequential model optimization (SMO) aims at discovering an input $x^* \in \mathcal{X}$ maximizing an objective function S :

$$x^* \in \arg \max_{x \in \mathcal{X}} S(x). \tag{5}$$

The SMO approach consists in tackling this problem by iteratively querying the objective function S in order to find a maximizer

RECOVER: sequential model optimization platform for combination drug repurposing identifies novel synergistic compounds *in vitro*

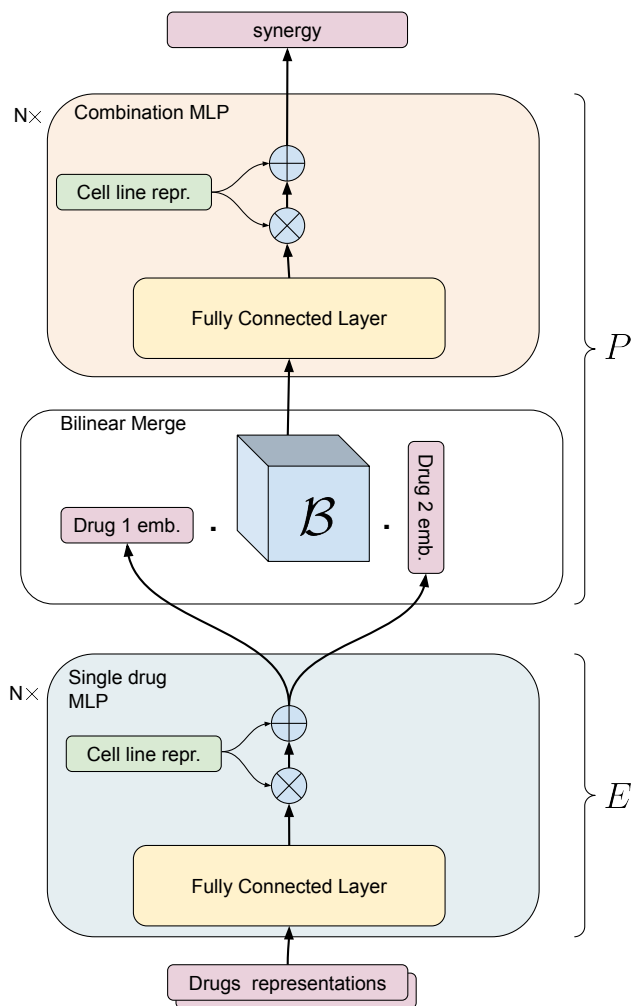


Figure 10: Overview of the RECOVER model. Drug representations are fed into the *Single drug module* which is composed of an MLP which can be conditioned on cell line. Given two drug embeddings, the synergy is predicted using the *Combination module*, composed of a bilinear operation followed by an MLP. The Combination MLP can be conditioned on cell line as well.

x^* in a minimal number of steps. At each step t , the dataset is augmented such that \mathcal{D}_t contains all the inputs that have already been acquired at time t . The dataset \mathcal{D}_t is then used to find the next query $x^{(t+1)}$. In the context of drug combinations, x corresponds to a pair of drugs, and the objective function S corresponds to the synergy score.

In what follows, f refers to an estimator of the objective function S . One may notice that several properties of the potential queries $x^{(t)}$ should be taken into account. One would like to find an $x^{(t)}$ that would be informative to acquire (i.e., the uncertainty at $x^{(t)}$ is high) in order to obtain a reliable estimator of the objective function

early on. On the other hand, one would like to find an $x^{(t)}$ that is a *good guess* in the sense that $f(x^{(t)})$ is close to the expected maximum $\max_{x \in \mathcal{X}} f(x)$. Looking for queries which are informative is referred to as *exploration* while looking for queries which are expected to maximize the objective function is called *exploitation*.

The key challenge of SMO is to balance between exploration and exploitation. This is typically achieved by designing an acquisition function α which defines a score on the space of inputs \mathcal{X} and takes into account both $f(x)$ and an estimate of the uncertainty at x . The input which maximizes the score α is chosen as the next query. An overview of the SMO approach is presented in Algorithm 1.

In our synthetic SMO experiments, the model was reinitialized and trained from scratch on all visible data after each query. Whilst not designed for optimal computational efficiency, this procedure ensures that the model is not overfitting on examples that have been acquired early on.

Algorithm 1: Sequential model optimization

Input: Initial data \mathcal{D}_0 , objective function estimator f
for $t \in \{1, 2, \dots\}$ **do**
 Select new $x^{(t+1)}$ by optimizing an acquisition function α

$$x^{(t+1)} = \arg \max_x \alpha(x; f)$$

 Query objective function S to obtain y^{t+1}
 Augment data $\mathcal{D}_{n+1} = \mathcal{D}_n \cup \{(x^{t+1}, y^{t+1})\}$
 Update estimator f
end for

Acquisition functions define the exploration strategy that is used to balance between exploration and exploitation. In what follows, we assume that we have access to an estimate of the mean of the predictive distribution, $\hat{\mu}(x)$, as well as an estimate of the uncertainty $\hat{\sigma}(x)$. The key acquisition functions considered are detailed below.

Brute-Force. $\alpha(x)$ corresponds to random noise, and therefore the drug combinations are selected at random.

Greedy. $\alpha(x) = \hat{\mu}(x)$. This acquisition function corresponds to pure exploitation whereby we select drug combinations with the highest predicted synergy.

Pure Exploration. $\alpha(x) = \hat{\sigma}(x)$. This acquisition function corresponds to pure exploration. The strategy aims at labelling the most informative examples in order to reduce model uncertainty as fast as possible, and corresponds to the traditional strategy in *Active Learning*.

Upper Confidence Bound (UCB). $\alpha(x) = \hat{\mu}(x) + \kappa \hat{\sigma}(x)$. This strategy balances between exploration and exploitation. $\kappa \in \mathbb{R}$ is a hyperparameter that is typically positive. Higher values of κ give more importance to exploration.

Unless specified otherwise, *in silico* experiments involving SMO were performed using UCB with $\kappa = 1$.

3.3 Recommendation generation

In order to generate the recommendations for *in vitro* experiments, we trained 3 models using 3 different seeds on the NCI-ALMANAC study, restricting ourselves to samples from the MCF7 cell line. We refer to these 3 models as pretrained.

Afterwards, we fine-tuned on *in-house* data. More precisely, the weights of one of the pretrained models were loaded, and some additional training was performed on *in-house* data only, using early stopping. This fine-tuning process was repeated with 12 different seeds for each pretrained model. We ended up with an ensemble of 36 fine-tuned models in total.

This ensemble was used to generate predictions ($\hat{\mu}, \hat{\sigma}$) for all candidate combinations. We then used UCB with $\kappa = 1$ to obtain a score according to which all candidates were ranked. The exact procedure to select the set of combinations for each of the three rounds is described in Subsection 2.3.

3.4 Dataset processing

Datasets have been pre-processed and normalized in a centralised data repository RESERVOIR¹.

The repository unifies data around biologically relevant molecules and their interactions. Pre-processing and normalizing scripts are provided for traceability, and a Python API has been made available to facilitate access. Below, the major data types included are briefly described.

3.4.1 Drugs. Data on drugs and biologically active compounds has been extracted from ChEMBL [29], pre-processed and indexed with unique identifiers. A translation engine has been provided such that a compound can be translated to a unique identifier using generic or brand drug names, SMILES strings and Pubchem [30] CIDs.

3.4.2 Cell Line Features. Additionally, RESERVOIR retrieved cell line features from the Cancer Dependency Map [31]. These include genetic mutations, base level gene expression and metadata.

3.4.3 Drug combinations. Literature drug combination data were extracted from DrugComb version 1.5 [20]. Quality control was applied on the experiments in DrugComb. Only blocks (i.e. combination matrices) complying to the following criteria were selected: (a.) filter out erroneous blocks that show very low variance, specifically inhibition standard deviation ≤ 0.05 , (b.) filter out small blocks less than 3×3 dimensions, (c.) filter out blocks with extreme inhibition values, such that $5\% < \text{mean pooled growth inhibition} < 95\%$.

The dataset used for model pretraining and *in silico* experiments consists of 4463 data points relative to experiments on MCF7 cell line expressed as max Bliss which were reported in the Almanac study. These data correspond to 4271 unique drug combinations made up by 95 unique drugs.

The prediction set for experiment selection was built by taking 54 out of the 95 Almanac drugs for which a mode of action (MoA) was annotated in ChEMBL 25 [29]. An additional 54 drugs were obtained by clustering 719 drugs with known MoA that are included in DrugComb but are not part of Almanac. Clustering was performed with the *k*-medoids algorithm as implemented in scikit-learn 0.24.2 [32] (`n_clusters=54`, `metric=Tanimoto similarity`,

`init=k-medoids++`), drugs were encoded by Morgan fingerprints with radius 2 and 1024 bits calculated with RDKit [33]. A representative compound for each cluster was obtained by taking the cluster centroid.

Three of the centroid drugs were replaced due to lack of availability from commercial vendors or due to poor reported solubility. Replacements for each of the three drugs were selected by taking the nearest analogue (evaluated by Tanimoto similarity) in the same cluster. 54 Almanac and 54 non-Almanac compounds thus selected were used to build a set of 2916 binary combinations made up by one Almanac and one non-Almanac compound.

3.5 Experimental protocol

3.5.1 Cell lines. MCF-7 cells were obtained from ATCC and maintained in DMEM (Corning) supplemented with 10% FBS (Corning) and Anti-anti (Gibco) at 37°C in 5% CO₂ in a humidified incubator. Before the screens, the cell lines were passaged twice after thawing. Cultures were confirmed to be free of mycoplasma infection using the MycoAlert Mycoplasma Detection Kit (Lonza).

3.5.2 Drug Combination Assays. A list of the tested compounds along with their concentration ranges and target mechanisms will be released with the full publication. The compound-specific concentration ranges were selected based on their published activities. All compounds were pre-diluted in DMSO to a stock concentration that varied from 10 to 50 mM, depending on the final concentration range required for each compound.

Briefly, compounds were plated as a 6×6 dose-response combination matrix in natural 384 well plates (Greiner), in a serial 1:3 dilutions of each agent (5 concentrations) and only DMSO as the lowest concentration. We used a combination plate layout where six compound pairs could be accommodated on one 384 well plate. A set of control wells with DMSO was included on all plates as negative control. To ensure reproducibility and comparability with the subsequent combination studies, the IC₅₀ of Doxorubicin was used as reference in a 6-point dose response format in each plate as positive (total killing) control.

Cells were seeded in white 384-well plates (Greiner) at 1000 cells/well in 50 μ L of media using a Multidrop dispenser and allowed to attach for 2 h. Compounds from pre-plated matrix plates were transferred to each well using a 100 nL head affixed to an Agilent Bravo automated liquid handling platform, and plates were incubated at 37°C in 5% CO₂ for an additional 72 hours. To measure the cell viability, CellTiter-Glo reagent (diluted 1:6 in water, Promega) was dispensed into the wells (30 μ L), incubated for 3 minutes, and luminescence was read on a Envision plate reader (Perkin-Elmer). Final DMSO concentration in assay wells was 0.2%. The assay was performed with 3 biological replicates.

4 DISCUSSION

We have presented the SMO toolbox RECOVER for drug combination selection. We demonstrated its potential through substantial benchmarking using publicly available databases, followed by prospective experimentation through a drug combination screen demonstrating an insightful proof of concept. We now provide commentary on key aspects on our approach covering datasets, computational methodology, and wet-lab techniques.

¹see <http://github.com/RECOVERcoalition/RESERVOIR>

RECOVER: sequential model optimization platform for combination drug repurposing identifies novel synergistic compounds *in vitro*

We note the considerable difficulties of working with biased publicly available datasets. Inconsistent media between multiple labs and the presence of spontaneous mutations within immortalised *in vitro* models limits ease of data integration between laboratories [34]. Within oncology, protein coding mutations may drive resistance to any one chemotherapeutic agent, but also large scale gene dosing changes from non-coding mutations [35], copy number variation [36] and aneuploidy [37]. These issues have been somewhat alleviated through careful choice of metric to optimise (max pooled Bliss synergy scores) and only using publicly available data for pretraining. Prospectively generated data using careful controls is only minimally affected by the aforementioned problems.

From a computational perspective, we experimented with a range of more complicated models. For example, we considered using graph neural networks to model biomolecular interactions [38], which have numerous benefits included greater biological interpretability and incorporation of prior knowledge, namely drug-target and protein-protein interactions. However, the computational overhead limited large hyper-parameter searches over the space of possible models – and ultimately only resulted in marginal increases in performance. We believe that the limited diversity of the dataset and the simplicity of the task, a one dimensional regression, did not allow these more advanced approaches to reach their full potential. Therefore, we prioritised a framework that could be run quickly for rapid turnaround of recommendations for experimental testing.

When considering active learning, we are required to collapse highly complex information into a single number to be optimised (i.e., a synergy score). Whilst there is opportunity to improve choices of metric (synergy scores may not reflect absolute cell viability), assay readouts that better characterise cell state (compared to cell viability) may provide a stronger starting point. In particular, an omic readout, through microarray [39] or single cell sequencing [40]; and high content imaging [41] provide a much higher dimensional understanding of cell state. Furthermore, derived properties from these readouts may be more interpretable, e.g., pathway activation [42] or extracellular signalling [43]. Remarkably, even while only using cell viability as a readout, we achieved significant progress in identifying novel synergistic drug combinations.

Drug combinations can achieve benefits that are unattainable by mono-therapies. For example, consider the case of certain blood cancers where multi-agent treatments can achieve cure rates of up to 80% [44], a significant improvement when compared to standard of care at the time. This calls for methods to significantly and robustly identify synergy in drug combinations – which we have developed here.

We showcase a general methodology, consisting of careful analysis of the properties of the machine learning pipeline – such as its *out-of-distribution* generalization capacities – to help us design some aspects of the *in vitro* experiments, and eventually ensure a smooth and successful interaction between the machine learning pipeline and the wet lab.

5 ACKNOWLEDGEMENTS

This research is funded in part by the Bill & Melinda Gates Foundation. The findings and conclusions contained within are those of

the authors and do not necessarily reflect positions or policies of the Bill & Melinda Gates Foundation. The authors would also like to thank Isabelle Lacroix for useful support.

REFERENCES

- [1] Adrian Schmid, Aline Wolfensberger, Johannes Nemeth, Peter W Schreiber, Hugo Sax, and Stefan P Kuster. Monotherapy versus combination therapy for multidrug-resistant gram-negative infections: Systematic review and meta-analysis. *Scientific reports*, 9(1):1–11, 2019.
- [2] Reza Bayat Mokhtari, Tina S Homayouni, Narges Baluch, Evgeniya Morgatskaya, Sushil Kumar, Bikul Das, and Herman Yeger. Combination therapy in combating cancer. *Oncotarget*, 8(23):38022, 2017.
- [3] João Delou, Alana SO Souza, Leonel Souza, and Helena L Borges. Highlights in resistance mechanism pathways for combination therapy. *Cells*, 8(9):1013, 2019.
- [4] Bissan Al-Lazikani, Udai Banerji, and Paul Workman. Combinatorial drug therapy for cancer in the post-genomic era. *Nature Biotechnology*, 30(7):679–692, July 2012.
- [5] Jeff Janes, Megan E Young, Emily Chen, Nicole H Rogers, Sebastian Burgstaller-Muehlbacher, Laura D Hughes, Melissa S Love, Mitchell V Hull, Kelli L Kuhen, Ashley K Woods, et al. The reframe library as a comprehensive drug repurposing library and its application to the treatment of cryptosporidiosis. *Proceedings of the National Academy of Sciences*, 115(42):10750–10755, 2018.
- [6] Rachel H Clare, Catherine Bardelle, Paul Harper, W David Hong, Ulf Börjesson, Kelly L Johnston, Matthew Collier, Laura Myhill, Andrew Cassidy, Darren Plant, et al. Industrial scale high-throughput screening delivers multiple fast acting macrofilaricides. *Nature communications*, 10(1):1–8, 2019.
- [7] Yadi Zhou, Fei Wang, Jian Tang, Ruth Nussinov, and Feixiong Cheng. Artificial intelligence in covid-19 drug repurposing. *The Lancet Digital Health*, 2020.
- [8] Yuriy Sverchkov and Mark Craven. A review of active learning approaches to experimental design for uncovering biological networks. *PLoS computational biology*, 13(6):e1005466, 2017.
- [9] Krishna C. Bulusu, Rajarshi Guha, Daniel J. Mason, Richard P. I. Lewis, Eugene Muratov, Yasaman Kalantar Motamedi, Murat Cokol, and Andreas Bender. Modelling of compound combination effects and applications to efficacy and toxicity: State-of-the-art, challenges and perspectives. *Drug Discovery Today*, 21(2):225–238, February 2016.
- [10] Adrià Cereto-Massagué, María José Ojeda, Cristina Valls, Miquel Mulero, Santiago Garcia-Vallvé, and Gerard Pujadas. Molecular fingerprint similarity search in virtual screening. *Methods*, 71:58–63, 2015.
- [11] Konrad J Karczewski and Michael P Snyder. Integrative omics for health and disease. *Nature Reviews Genetics*, 19(5):299, 2018.
- [12] Feixiong Cheng, István A Kovács, and Albert-László Barabási. Network-based prediction of drug combinations. *Nature communications*, 10(1):1–11, 2019.
- [13] Michael P Menden, Dennis Wang, Mike J Mason, Bence Szalai, Krishna C Bulusu, Yuanfang Guan, Thomas Yu, Jaewoo Kang, Minji Jeon, Russ Wolfinger, et al. Community assessment to advance computational prediction of cancer drug combinations in a pharmacogenomic screen. *Nature communications*, 10(1):1–17, 2019.
- [14] Marinika Zitnik, Monica Agrawal, and Jure Leskovec. Modeling polypharmacy side effects with graph convolutional networks. *Bioinformatics*, 34(13):i457–i466, 2018.
- [15] Andreea Deac, Yu-Hsiang Huang, Petar Veličković, Pietro Liò, and Jian Tang. Drug-drug adverse effect prediction with graph co-attention. *arXiv preprint arXiv:1905.00534*, 2019.
- [16] Kristina Preuer, Richard PI Lewis, Sepp Hochreiter, Andreas Bender, Krishna C Bulusu, and Günter Klambauer. Deep synergy: predicting anti-cancer drug synergy with deep learning. *Bioinformatics*, 34(9):1538–1546, 2018.
- [17] Wengong Jin, Jonathan M Stokes, Richard T Eastman, Zina Itkin, Alexey V Zakharov, James J Collins, Tommi S Jaakkola, and Regina Barzilay. Deep learning identifies synergistic drug combinations for treating covid-19. *Proceedings of the National Academy of Sciences*, 118(39), 2021.
- [18] Benedek Rozemberczki, Anna Gogoleva, Sebastian Nilsson, Gavin Edwards, Andriy Nikolov, and Eliseo Papa. Moomin: Deep molecular omics network for anti-cancer drug combination therapy. *arXiv preprint arXiv:2110.15087*, 2021.
- [19] Brian Hie, Bryan D Bryson, and Bonnie Berger. Leveraging uncertainty in machine learning accelerates biological discovery and design. *Cell Systems*, 11(5):461–477, 2020.
- [20] Bulat Zagidullin, Jehad Aldahdooh, Shuyu Zheng, Wenyu Wang, Yinyin Wang, Joseph Saad, Alina Malyutina, Mohieddin Jafari, Ziaurrehman Tanoli, Alberto Pessia, et al. Drugcomb: an integrative cancer drug combination data portal. *Nucleic acids research*, 47(W1):W43–W51, 2019.
- [21] A Žilinskas and J Mockus. On a bayes method for seeking an extremum. *Automatika i vyчисlitel'naja tekhnika*, (3), 1972.
- [22] Susan L Holbeck, Richard Camalier, James A Crowell, Jeevan Prasaad Govindharajulu, Melinda Hollingshead, Lawrence W Anderson, Eric Polley, Larry Rubinstein,

- Apurva Srivastava, Deborah Wilsker, et al. The National Cancer Institute AL-MANAC: a comprehensive screening resource for the detection of anticancer drug pairs with enhanced therapeutic activity. *Cancer Research*, 77(13):3564–3576, 2017.
- [23] Jennifer O’Neil, Yair Benita, Igor Feldman, Melissa Chenard, Brian Roberts, Yaping Liu, Jing Li, Astrid Kral, Serguei Lejnine, Andrey Loboda, et al. An unbiased oncology compound screen to identify novel combination strategies. *Molecular Cancer Therapeutics*, 15(6):1155–1162, 2016.
- [24] Harry L Morgan. The generation of a unique machine description for chemical structures—a technique developed at chemical abstracts service. *Journal of Chemical Documentation*, 5(2):107–113, 1965.
- [25] Ethan Perez, Florian Strub, Harm De Vries, Vincent Dumoulin, and Aaron Courville. Film: Visual reasoning with a general conditioning layer. In *Proceedings of the AAAI Conference on Artificial Intelligence*, volume 32, 2018.
- [26] Hiral A Shah, James H Fischer, Neeta K Venepalli, Oana C Danciu, Sonia Christian, Meredith J Russell, Li C Liu, James P Zacny, and Arkadiusz Z Dudek. Phase I study of aurora a kinase inhibitor alisertib (mln8237) in combination with selective vegfr inhibitor pazopanib for therapy of advanced solid tumors. *American journal of clinical oncology*, 42(5):413–420, 2019.
- [27] Balaji Lakshminarayanan, Alexander Pritzel, and Charles Blundell. Simple and scalable predictive uncertainty estimation using deep ensembles, 2017.
- [28] Moksh Jain, Salem Lahlou, Hadi Nekoei, Victor Butoi, Paul Bertin, Jarrid Rector-Brooks, Maksym Korablyov, and Yoshua Bengio. DEUP: direct epistemic uncertainty prediction. *CoRR*, abs/2102.08501, 2021.
- [29] Mark Davies, Michał Nowotka, George Papadatos, Nathan Dedman, Anna Gaulton, Francis Atkinson, Louisa Bellis, and John P Overington. ChEMBL web services: streamlining access to drug discovery data and utilities. *Nucleic Acids Research*, 43(W1):W612–W620, 2015.
- [30] Sunghwan Kim, Jie Chen, Tiejun Cheng, Asta Gindulyte, Jia He, Siqian He, Qingliang Li, Benjamin A Shoemaker, Paul A Thiessen, Bo Yu, et al. Pubchem 2019 update: improved access to chemical data. *Nucleic acids research*, 47(D1):D1102–D1109, 2019.
- [31] Mahmoud Ghandi, Franklin W. Huang, Judit Jané-Valbuena, Gregory V. Kryukov, Christopher C. Lo, E. Robert McDonald, Jordi Barretina, Ellen T. Gelfand, Craig M. Bielski, Haoxin Li, Kevin Hu, Alexander Y. Andreev-Drakhlin, Jaegil Kim, Julian M. Hess, Brian J. Haas, François Aguet, Barbara A. Weir, Michael V. Rothberg, Brenton R. Paolella, Michael S. Lawrence, Rehan Akbani, Yiling Lu, Hong L. Tiv, Prafulla C. Gokhale, Antoine de Weck, Ali Amin Mansour, Coyin Oh, Juliann Shih, Kevin Hadi, Yanay Rosen, Jonathan Bistline, Kavitha Venkatesan, Anupama Reddy, Dmitriy Sonkin, Manway Liu, Joseph Lehar, Joshua M. Korn, Dale A. Porter, Michael D. Jones, Javad Golji, Giordano Caponigro, Jordan E. Taylor, Caitlin M. Dunning, Amanda L. Creech, Allison C. Warren, James M. McFarland, Mahdi Zamanighomi, Audrey Kauffmann, Nicolas Stransky, Marcin Imielinski, Yosef E. Maruvka, Andrew D. Cherniack, Aviad Tsherniak, Francisca Vazquez, Jacob D. Jaffe, Andrew A. Lane, David M. Weinstock, Cory M. Johannessen, Michael P. Morrissey, Frank Stegmeier, Robert Schlegel, William C. Hahn, Gad Getz, Gordon B. Mills, Jesse S. Boehm, Todd R. Golub, Levi A. Garraway, and William R. Sellers. Next-generation characterization of the Cancer Cell Line Encyclopedia. *Nature*, 569(7757):503–508, May 2019.
- [32] F. Pedregosa, G. Varoquaux, A. Gramfort, V. Michel, B. Thirion, O. Grisel, M. Blondel, P. Prettenhofer, R. Weiss, V. Dubourg, J. Vanderplas, A. Passos, D. Cournapeau, M. Brucher, M. Perrot, and E. Duchesnay. Scikit-learn: Machine learning in Python. *Journal of Machine Learning Research*, 12:2825–2830, 2011.
- [33] RDKit: Open-source cheminformatics. <http://www.rdkit.org>.
- [34] Cordula Hirsch and Stefan Schildknecht. In vitro research reproducibility: Keeping up high standards. *Frontiers in pharmacology*, 10:1484, 2019.
- [35] Ziga Avsec, Vikram Agarwal, Daniel Visentin, Joseph R Ledsam, Agnieszka Grabska-Barwinska, Kyle R Taylor, Yannis Assael, John Jumper, Pushmeet Kohli, and David R Kelley. Effective gene expression prediction from sequence by integrating long-range interactions. *bioRxiv*, 2021.
- [36] Xin Shao, Ning Lv, Jie Liao, Jinbo Long, Rui Xue, Ni Ai, Donghang Xu, and Xiaohui Fan. Copy number variation is highly correlated with differential gene expression: a pan-cancer study. *BMC medical genetics*, 20(1):1–14, 2019.
- [37] Jake P Taylor-King. Rethinking rare disease: longevity-enhancing drug targets through x-linked aneuploidy. *Trends in Genetics*, 2021.
- [38] Thomas Gaudelot, Ben Day, Arian R Jamasb, Jyothish Soman, Cristian Regep, Gertrude Liu, Jeremy BR Hayter, Richard Vickers, Charles Roberts, Jian Tang, et al. Utilizing graph machine learning within drug discovery and development. *Briefings in bioinformatics*, 22(6):bbab159, 2021.
- [39] Aravind Subramanian, Rajiv Narayan, Steven M Corsello, David D Peck, Ted E Natoli, Xiaodong Lu, Joshua Gould, John F Davis, Andrew A Tubelli, Jacob K Asiedu, et al. A next generation connectivity map: L1000 platform and the first 1,000,000 profiles. *Cell*, 171(6):1437–1452, 2017.
- [40] Haide Chen, Yuan Liao, Guodong Zhang, Zhongyi Sun, Lei Yang, Xing Fang, Huiyu Sun, Lifeng Ma, Yuting Fu, Jingyu Li, et al. High-throughput microwell-seq 2.0 profiles massively multiplexed chemical perturbation. *Cell discovery*, 7(1):1–4, 2021.
- [41] Mark-Anthony Bray, Shantanu Singh, Han Han, Chadwick T Davis, Blake Borgeson, Cathy Hartland, Maria Kost-Alimova, Sigrun M Gustafsdottir, Christopher C Gibson, and Anne E Carpenter. Cell painting, a high-content image-based assay for morphological profiling using multiplexed fluorescent dyes. *Nature protocols*, 11(9):1757–1774, 2016.
- [42] Tuan-Minh Nguyen, Adib Shafi, Tin Nguyen, and Sorin Draghici. Identifying significantly impacted pathways: a comprehensive review and assessment. *Genome biology*, 20(1):1–15, 2019.
- [43] Jake P Taylor-King, Etienne Baratchart, Andrew Dhawan, Elizabeth A Coker, Inga Hansine Rye, Hege Russnes, S Jon Chapman, David Basanta, and Andriy Marusyk. Simulated ablation for detection of cells impacting paracrine signalling in histology analysis. *Mathematical medicine and biology: a journal of the IMA*, 36(1):93–112, 2019.
- [44] Emil Frei. Curative Cancer Chemotherapy. *Cancer Research*, 45(12 Part 1):6523–6537, December 1985.

APPENDIX

A MODEL SELECTION

A.1 Hyperparameter tuning

RECOVER. The hyperparameters of RECOVER have been optimized within the following set of values. Because it was not tractable to perform a grid search over all possible values at once, hyperparameters have been optimized one at a time in an iterative way. The set of parameters that yielded best performance is highlighted.

- Learning rate: [1×10^{-1} , 1×10^{-2} , 1×10^{-3} , **1×10^{-4}** , 1×10^{-5} , 1×10^{-6}]
- Batch size: [16, 32, 64, **128**, 256]
- Weight decay: [1 , 1×10^{-1} , 1×10^{-2} , 1×10^{-3} , 1×10^{-4} , 1×10^{-5} , 1×10^{-6} , 0]
- Morgan fingerprint radius: [2, 3, 4, 5]
- Morgan fingerprint dimension: [**1024**, 2048]
- Output dimension of the single drug MLP: [16, 32, 64, **128**, 256]
- Dimension(s) of the hidden layer(s) of the single drug MLP: [[512], [256], [**1024**], [2048], [4096], [1024, 1024], [1024, 1024, 1024], [1024, 512], [1024, 512, 256]]
- Dimension(s) of the hidden layer(s) of the combination MLP: [[32], [**64**], [128], [256], [64, 16], [64, 32], [64, 64]]

Baselines. A grid search has been performed to optimize the hyperparameters of *Gradient Boosting Trees*. The set of parameters that yielded best performance is highlighted. The number of trees was set to 100.

- Maximum tree depth: [2, 5, 10, **20**]
- Minimum number of samples to split a node: [2, 5, 10, **20**, 50]
- Learning rate: [0.0001, 0.001, 0.01, **0.1**, 1]
- Maximum feature: [all, $\sqrt{\text{total number of features}}$, $\log_2[\text{total number of features}]$]

Similarly, a grid search has been performed for *Linear SVM*:

- tolerance for stopping criterion: [1×10^{-1} , 1×10^{-2} , **1×10^{-3}** , 1×10^{-4} , 1×10^{-5}]
- Regularization C: [0.0001, 0.001, 0.01, **0.1**, 1., 10]

A.2 Feature importance study

In Table 3, we compare the performance of RECOVER when provided with different types of features for the drugs. Interestingly, the performance of the model is similar whether the one hot encoding of the drug or its Morgan fingerprint is used as input. We notice a slight improvement when using both feature types together.

Note that the number of parameters of the model is always the same regardless of the type of feature provided as input. When a feature type should not be used, the corresponding part of the drug feature vector is set to zero without changing its dimension.

Table 3: Feature importance study for the prediction of max Bliss score on the MCF7 cell line. Standard deviation computed over 3 seeds.

	R^2	Spearman corr.
RECOVER (fingerprint + one hot)	0.242 ± 0.006	0.466 ± 0.007
RECOVER (fingerprint)	0.232 ± 0.007	0.458 ± 0.010
RECOVER (one hot)	0.230 ± 0.029	0.449 ± 0.017

B THEORETICAL UPPER BOUNDS

In this section, we investigate in more details the reasons why RECOVER achieves relatively poor performance in terms of Spearman correlation and R^2 , while yielding significant speed-up in the Sequential Model optimization setting.

Several things might prevent our model from achieving high performance on the synergy score regression task. First, the data acquisition process is noisy. Second, the distribution of maximum Bliss synergy scores is highly non uniform: most of the data points are close to zero, while some examples are very far from the mean.

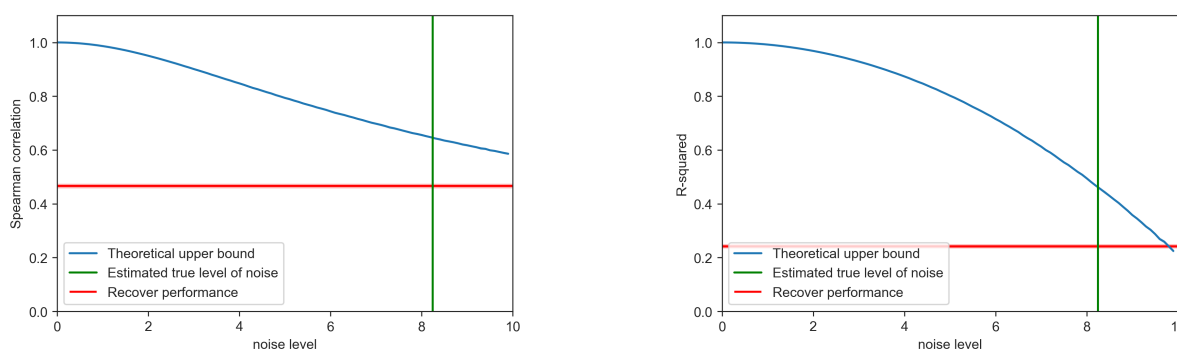
As an example, let us consider the case of Spearman correlation. Given that the observations are noisy, the observed rank among synergies might be corrupted compared to the *true* one, especially in the region close to zero where the density of examples is very high. The tails of the distribution represent a very small percentage of the total number of examples, and thus have a little effect on the value of the aggregated statistics.

For these reasons, aggregated statistics may not capture well what we care about. In order to get a better understanding of the performance of our model, we wanted to compare aggregated statistics to their theoretical upper bound, taking into account the presence of noise and the distribution of synergy scores.

Evaluating the level of noise. We first evaluated the level of noise by considering all the replicates from the NCI-ALMANAC study. Two examples are considered replicates when the same pair of drugs has been tested on the same cell line. We found 1960 triplets ($\{\text{drug1}, \text{drug2}\}$, cell line) that had been tested several times. For each triplet, we computed the standard deviation of the maximum Bliss score across the replicates. Let us call this the level of noise for a given triplet. We then computed the average level of noise \bar{N} across all triplets.

Evaluating the performance of a perfect regressor model as a function of the level of noise in the dataset. In order to simulate the performance of a perfect regressor model, we considered the synergies from NCI-ALMANAC as the *true* synergies. We then simulated a noisy acquisition process by corrupting the *true* synergies with some Gaussian noise $\mathcal{N}(0, \sigma = \bar{N})$. The upper bound was then obtained by computing the aggregated statistics between the *true* synergies and the corrupted ones. This corresponds to evaluating on the *true* synergies a model which fits perfectly the noisy observations.

Upper bounds have been computed for R^2 and Spearman correlation using various levels of noise and are reported in Figure 11. While there is still room for improvement for RECOVER, we see that the noisy acquisition process alone leads to significant limitations in the performance that can be reached.



(a) Theoretical upper bound for the Spearman correlation as a function of the level of noise in the measurement (b) Theoretical upper bound for the R^2 as a function of the level of noise in the measurement

Figure 11: Comparison of the performance of RECOVER with theoretical upper bounds that take into account the level of noise in the data. The upper bound, shown in blue, is a function of the level of noise. The standard deviation for the upper bound is lower than $\times 10^{-3}$ for both statistics (estimated over 3 seeds). The estimated level of noise in our dataset is shown in green. The performance of RECOVER as well as its standard error are shown in red.

C MODEL EVALUATION

C.1 Visualization of drug embeddings

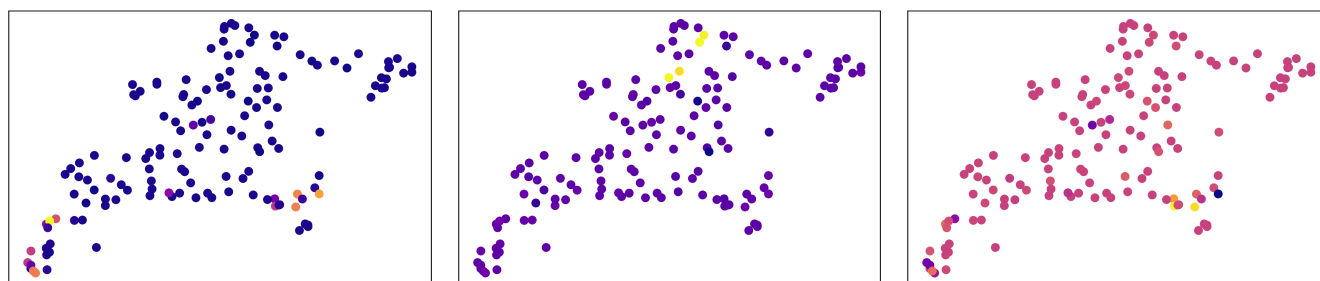
As an attempt to get a better insight into the drug embeddings learnt by RECOVER, we report UMAP visualizations of the drug embeddings generated by the *single drug* module. Color represents information about the known targets of each drug, which is not used by the RECOVER model.

As shown in Figure 12, there seems to be some consistency between the drug embeddings learnt by RECOVER and the known targets of the drugs. Drugs with similar targets tend to form one or several clusters.

For each single drug in the NCI-ALMANAC dataset, we gathered its targets from the ChEMBL database, and obtained a binary vector representation for each drug. We then computed a PCA decomposition on these target-information binary vectors, which gave us a 3-dimensional vector v for each drug. v summarizes what is known about the Mechanism of Action of the drug.

We show the values of the vectors v as color in three different plots, the first plot corresponding to the first dimension and so on.

RECOVER: sequential model optimization platform for combination drug repurposing identifies novel synergistic compounds *in vitro*



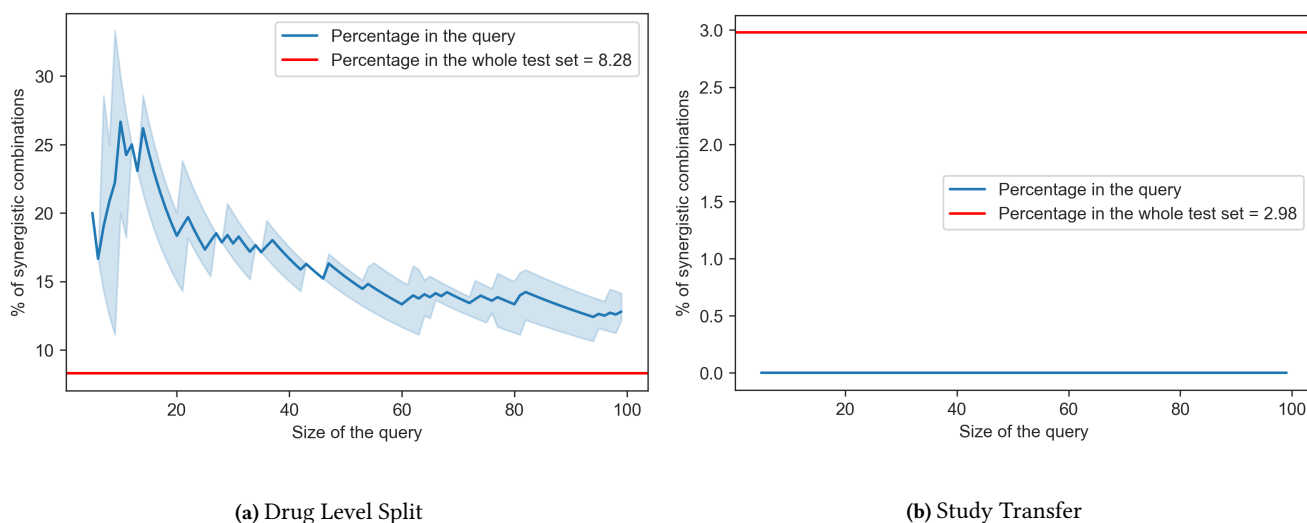
(a) Component 1

(b) Component 2

(c) Component 3

Figure 12: UMAP visualization of the single drug embeddings (output of the single drug MLP) learnt by RECOVER. Colors represent the first three components of a PCA decomposition of drug-target information obtained from the ChEMBL database. While RECOVER did not use any drug target information, there seems to be some consistency between the drug embeddings learnt by RECOVER and the known targets of the drugs. Drugs with similar targets tend to form one or several clusters.

C.2 Proportion of synergistic combinations in query



(a) Drug Level Split

(b) Study Transfer

Figure 13: Proportion of highly synergistic combinations (synergy score > 30) in queried combinations using RECOVER as a function of the size of the query. **(a) Drug Level Split.** The percentage in the query is superior to the percentage of synergistic combinations in the whole test set, meaning that the model performs better than the level of randomness. **(b) Study Transfer.** The percentage in the query is below to the percentage of synergistic combinations in the whole test set, meaning that the model performs worse than the level of randomness. Standard deviation computed over 3 seeds.

D SEQUENTIAL MODEL OPTIMIZATION

D.1 Comparison of the different acquisition functions

When simulating the context of the *in vitro* experiments, we did not notice any difference in performance between the two Model-based acquisition functions Greedy and UCB. However, in another context, we noticed some benefits of taking into account uncertainty into the exploration strategy.

In the following experiments, uncertainty was directly estimated using an *uncertainty predictor*, and the task is the prediction of the average Bliss synergy score (instead of maximum Bliss), which corresponds to the average over the dose-response matrix of the concentration specific Bliss scores. 5 combinations were acquired at a time, instead of 30. Only the MCF7 cell line was used.

As shown in Figure 14, UCB outperforms Greedy acquisition, demonstrating the value of taking uncertainty into account to guide experiments in that context.

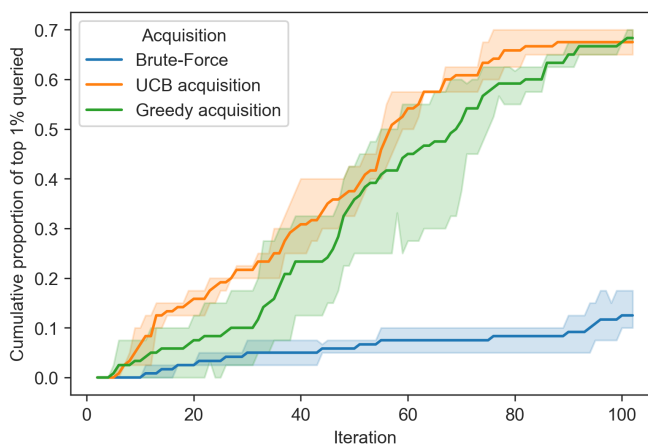


Figure 14: Cumulative proportion of the top 1% synergistic combinations that have been discovered by the SMO pipeline along SMO iterations. UCB outperforms Greedy acquisition. 5 combinations acquired at a time. Uncertainty estimated using direct uncertainty estimation. Standard deviation computed over 3 seeds.

D.2 Effect of pretraining

While we saw in Table 2 that RECOVER does not generalize well *without adaptation* to new experimental settings, remarkably, knowledge can still be transferred from one experimental setting to another. More precisely, pretraining our models on O’Neil improved performance of the SMO pipeline on the NCI-ALMANAC study, as shown in Figure 15.

In these experiments, we restricted ourselves to cell lines which were covered in both the O’Neil and NCI-ALMANAC studies. The model was first pretrained on the O’Neil study. After that, we simulated the SMO process on the subset of NCI-ALMANAC consisting of drug pairs for which at least one of the drugs was included in the O’Neil study. We compared against a model that had not been pretrained.

All models were conditioned on cell line, and two different uncertainty estimation methods were tested. UCB acquisition was used.

As the MCF7 cell line is not included in the O’Neil study, we could not restrict ourselves to MCF7 as usual. Instead, we performed SMO on all cell lines at the same time, resulting in a space of possible queries which is bigger than in other experiments where only MCF7 was used. This explains why the rate of discovery is slower in this case.

RECOVER: sequential model optimization platform for combination drug repurposing identifies novel synergistic compounds *in vitro*

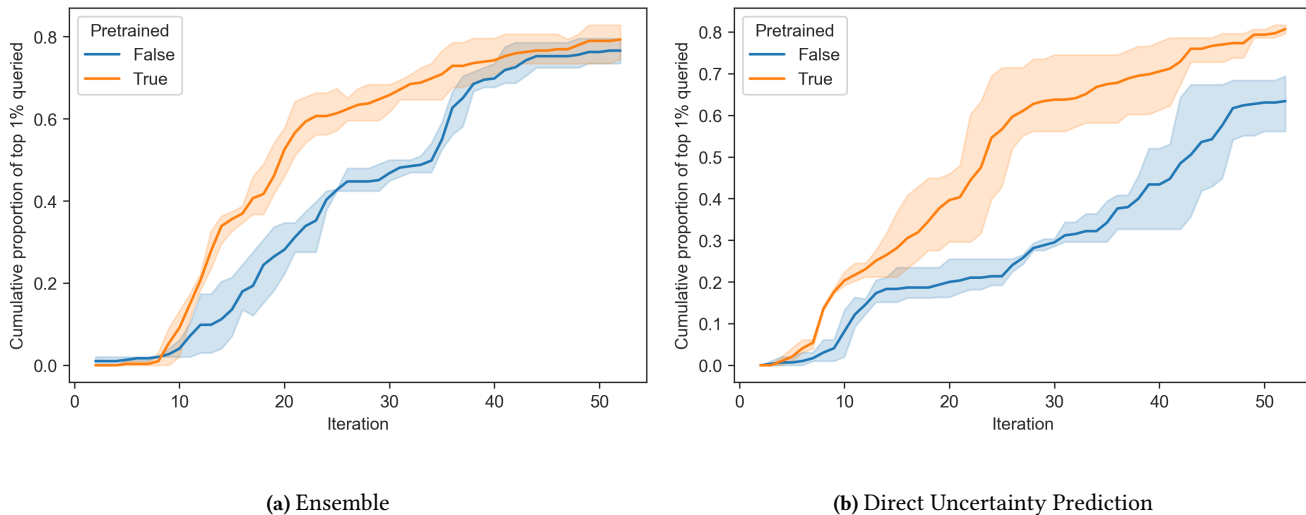


Figure 15: Effect of pretraining on the rate of discovery of highly synergistic combinations. The model that has been pretrained on O’Neil outperforms the other model, initialized randomly. Experiments on the subset of NCI-ALMANAC consisting of drug pairs for which at least one of the drugs is included in O’Neil. Using UCB acquisition with either (a) Ensemble or (b) Direct Uncertainty Estimation. Standard deviation computed over 3 seeds.

E DERIVATION OF THE NEGATIVE LOG LIKELIHOOD CRITERION

The uncertainty model predicts $\hat{\sigma}$, the standard deviation of the predictive uncertainty, which is different for every example in the dataset. For each combination, given the expected synergy $\hat{\mu}$ predicted by the mean predictor, and the actual observation y , we wish to find $\hat{\sigma}$ that maximizes the probability of y assuming a predictive distribution of the form $\mathcal{N}(\hat{\mu}, \hat{\sigma})$.

$$\log p(y|\hat{\mu}, \hat{\sigma}) = \log \left[\frac{1}{\sqrt{2\pi}\hat{\sigma}^2} e^{-\frac{1}{2}\left(\frac{y-\hat{\mu}}{\hat{\sigma}}\right)^2} \right] \tag{6}$$

$$= -\frac{1}{2} \log(2\pi) - \frac{1}{2} \log(\hat{\sigma}^2) - \frac{1}{2} \frac{(y - \hat{\mu})^2}{\hat{\sigma}^2} \tag{7}$$

Therefore, maximizing $\log p(y|\hat{\mu}, \hat{\sigma})$ w.r.t. $\hat{\sigma}$ is equivalent to minimizing the following criterion: $NLL = \frac{1}{2} \log(\hat{\sigma}^2) + \frac{1}{2} \frac{(y-\hat{\mu})^2}{\hat{\sigma}^2}$. Note that only the DEUP uncertainty predictor is trained using this criterion. The mean predictor is trained using Mean Square Error (MSE) as we found experimentally that it was more stable.